

Diffuse Interface Methods for Multiple Phase Materials: An Energetic Variational Approach

J. Brannick^{1,*}, C. Liu¹, T. Qian², and H. Sun¹

¹ *Department of Mathematics, The Pennsylvania State University, University Park, PA 16802, USA.*

² *Hong Kong University of Science and Technology, Clear Water Bay, Kowloon Hong Kong.*

Abstract. In this paper, we introduce a diffuse interface model for describing the dynamics of mixtures involving multiple (two or more) phases. The coupled hydrodynamical system is derived through an energetic variational approach. The total energy of the system includes the kinetic energy and the mixing (interfacial) energies. The least action principle (or the principle of virtual work) is applied to derive the conservative part of the dynamics, with a focus on the reversible part of the stress tensor arising from the mixing energies. The dissipative part of the dynamics is then introduced through a dissipation function in the energy law, in line with the Onsager principle of least energy dissipation. The final system, formed by a set of coupled time-dependent partial differential equations, reflects a balance among various conservative and dissipative forces and governs the evolution of velocity and phase fields. To demonstrate the applicability of the proposed model, a few two-dimensional simulations have been carried out, including (1) the force balance at the three-phase contact line in equilibrium, (2) a rising bubble penetrating a fluid-fluid interface, and (3) a solid particle falling in a binary fluid. The effects of slip at solid surface have been examined in connection with contact line motion and a pinch-off phenomenon.

AMS subject classifications: 65F10, 65N22, 65N55

Key words: multiphase flow, energetic variational approach

1. Introduction

Phase field methods (PFM), also known as diffuse interface methods, have been widely used in modeling two-phase problems and free interface motion of mixtures. The methods are based on a labeling function $\phi(x)$, which usually takes values as ± 1 , to distinguish between the two different materials (phases). Du et. al. applied phase field methods in their studies of the configurations and the deformations of elastic bio-membranes [5]. Liu and Shen investigated the use of two-phase models for studying bubble relaxation, rise, and coalescence [16]. Qian et al. studied the moving contact line problem using phase field methods in [17]. Yue et.

*Corresponding author. *Email addresses:* brannick@psu.edu (J. Brannick), liu@math.psu.edu (C. Liu), tmaqian@ust.hk (T. Qian), sun@math.psu.edu (H. Sun)

al. [23] studied a general approach for modeling two-phase complex fluids, with numerical examples simulating emulsion of nematic drops in a Newtonian matrix. Recently Shen and Yang applied the phase field method to two-phase incompressible flows with different densities and viscosities [20].

The basic idea of the two-phase PFM is to use a coarse graining (mean field) model to describe the microscopic dynamics of the mixtures. In the hydrodynamical (macroscopic) time scale, such dynamics involve the deformations of each phase, the interaction between the two, and their interactions with the surrounding environment. The underlying dynamical system is derived from applying variational principles to a certain free energy, e.g. the classical Ginzburg-Landau type energy [3]

$$\mathcal{F}_{CH} = \int \gamma \left\{ \frac{\varepsilon}{2} |\nabla \phi|^2 + \frac{1}{4\varepsilon} (\phi^2 - 1)^2 \right\} dx,$$

where $\phi(x)$ is the phase field function and ε is the width of the diffuse interface. The two parts in the above integrand represent the ‘‘philic’’ and ‘‘phobic’’ interactions between the two materials. The parameter γ can be associated to the surface tension in the conventional sharp interface formulations. The applicability of this model has been demonstrated for many different applications (see [6] [7] [18] and references therein). Although analytically it is still an open question whether the sharp interface model can be recovered by the phase field model via a rigorous proof, the latter has been applied theoretically and numerically for a long time. Moreover, from a practical and more physical point of view, the sharp interface models can be viewed as the simplification or idealization of phase field models.

In this paper, we show that for problems in which more than two phases are involved, we can introduce additional labeling functions to distinguish among them, as illustrated in Figure 1. The derivation follows from applying the energetic variational framework as in [16, 23]. Here, in the region at the bottom of the figure, a single phase is characterized by $\{\psi = 1\}$ and ϕ is not defined. In the top region of the figure, there are two phases distinguished by different values of ϕ , while sharing the same ψ value. In a similar way, four different phases can be characterized by two phase field functions. We note that such an approach has been considered in other contexts [2].

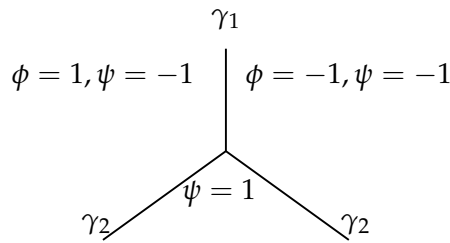


Figure 1: A Schematic illustration for three phases distinguished/labelled by two phase fields ϕ and ψ .

The remaining sections of the paper are organized as follows. We derive our multi-phase model using a variational approach in Section 2. In Section 3, we discuss the numerical meth-

ods in our simulations and present results for a variety of 2d multi-phase applications. Section 4 presents concluding remarks and future work.

2. Derivation of multi-phase model

In analogy to approaches used for modeling two-phase problems [16], for multi-phase problems we define a mixing energy

$$E = \int_{\Omega} W(\phi, \nabla\phi, \psi, \nabla\psi) dx = \int_{\Omega} \left\{ \gamma_1 \left(\frac{\psi-1}{2} \right)^2 \left(\frac{\varepsilon_1}{2} |\nabla\phi|^2 + \frac{1}{4\varepsilon_1} (\phi^2 - 1)^2 \right) + \gamma_2 \left(\frac{\varepsilon_2}{2} |\nabla\psi|^2 + \frac{1}{4\varepsilon_2} (\psi^2 - 1)^2 \right) \right\} dx, \quad (2.1)$$

where ε_1 and ε_2 are the widths of the interfaces along the differing phases and γ_1 and γ_2 are the surface tensions at the interfaces. The $\left(\frac{\psi-1}{2}\right)^2$ coefficient in the energy density for ϕ is used to ensure that interactions between two different phases (labeled as $\phi = 1, \psi = -1$ and $\phi = -1, \psi = -1$) do not directly influence the bulk of the third phase (labeled as $\psi = 1$). We assume both γ_1 and γ_2 are constants, although in general the parameters $\varepsilon_i, \gamma_i, i = 1, 2$ can be taken to be phase-dependent.

Here we want to stress the relation of our approach to other related treatments by other groups, such as those by Kim and Lowengrub [10, 12]. It is clear, one needs at least 2 phase field functions to label the 3 distinct materials. The key difference, and hence one of the main difficulties, is in the choices of the free energy functionals. While the free energy functionals in [10, 12] are nondegenerate, the free energy in (2.1) involves degeneracy for the region $\{x : \psi = 1\}$. This generic degeneracy stands for the physics that in this solid region, there is no effects from the fluids interactions (due to the dynamics of ϕ).

Next, by adding the fluid equations to the system, we obtain the total energy of the hydrodynamic system as a weighted sum of the kinetic energy and the mixing energy

$$\mathcal{E} = \int_{\Omega} \left(\frac{1}{2} \rho |u|^2 + \lambda W(\phi, \nabla\phi, \psi, \nabla\psi) \right) dx.$$

Here, the constant λ measures the competition between the two types of energy. To derive the stress tensor from the Ginzburg-Landau energy we apply the principle of virtual work (PoVW) [4], which states that the virtual work of the elastic energy

$$E = \int_{\Omega} W(\phi, \nabla\phi, \psi, \nabla\psi)$$

due to a virtual displacement δx is given by

$$\delta E = \int_{\Omega} \sigma : \nabla \delta x dx = - \int_{\Omega} (\nabla \cdot \sigma) \cdot \delta x dx. \quad (2.2)$$

Before calculating the left-hand side in (2.2), we take the macroscopic kinematic assumption of both ϕ and ψ being convective only, i.e, there is no relaxation which contributesto the microscopic internal dissipation:

$$\begin{aligned} \phi_t + u \cdot \nabla \phi &= 0, & \psi_t + u \cdot \nabla \psi &= 0. \\ \Rightarrow \delta \phi + \delta x \cdot \nabla \phi &= 0, & \delta \psi + \delta x \cdot \nabla \psi &= 0. \end{aligned} \quad (2.3)$$

Taking the gradient of the two equations in (2.3) gives

$$\begin{aligned}\delta \nabla \phi + (\nabla \delta x)^T \nabla \phi + (D^2 \phi) \delta x &= 0, \\ \delta \nabla \psi + (\nabla \delta x)^T \nabla \psi + (D^2 \psi) \delta x &= 0,\end{aligned}$$

where $D^2 \phi$ is the Hessian of ϕ .

The virtual work can then be calculated as follows:

$$\begin{aligned}\delta E &= \int_{\Omega} \left(\frac{\partial W}{\partial \phi} \cdot \delta \phi + \frac{\partial W}{\partial \nabla \phi} : \delta \nabla \phi + \frac{\partial W}{\partial \psi} \cdot \delta \psi + \frac{\partial W}{\partial \nabla \psi} : \delta \nabla \psi \right) dx \\ &= \int_{\Omega} \gamma_1 \left(\frac{\psi - 1}{2} \right)^2 \frac{(\phi^2 - 1)\phi}{\varepsilon_1^2} (-\delta x \cdot \nabla \phi) dx + \int_{\Omega} \gamma_1 \left(\frac{\psi - 1}{2} \right)^2 [-(\nabla \delta x)^T \nabla \phi - (D^2 \phi) \delta x] dx \\ &\quad + \int_{\Omega} \gamma_2 \left\{ \frac{(\psi^2 - 1)\psi}{\varepsilon_2^2} + \frac{\psi - 1}{2} \left[\frac{1}{2} |\nabla \phi|^2 + \frac{1}{4\varepsilon_1} (\phi^2 - 1) \right] \right\} (-\delta x \cdot \nabla \psi) dx \\ &\quad + \int_{\Omega} \gamma_2 \nabla \psi [-(\nabla \delta x)^T \nabla \psi - (D^2 \psi) \delta x] dx \\ &= - \int_{\Omega} \gamma_1 \left(\frac{\psi - 1}{2} \right)^2 \nabla \frac{(\phi^2 - 1)^2}{4\varepsilon_1^2} \delta x - \int_{\Omega} \gamma_1 \left[\left(\frac{\psi - 1}{2} \right)^2 \nabla \phi \otimes \nabla \phi \right] \nabla \delta x dx \\ &\quad - \int_{\Omega} \gamma_1 \left(\frac{\psi - 1}{2} \right)^2 \nabla \frac{|\nabla \phi|^2}{2} \delta x dx - \int_{\Omega} \nabla \frac{(\psi^2 - 1)^2}{4\varepsilon_2^2} \delta x dx \\ &\quad - \int_{\Omega} \gamma_2 \nabla \left[\left(\frac{\psi - 1}{2} \right)^2 \right] \left[\frac{1}{2} |\nabla \phi|^2 + \frac{1}{4\varepsilon_1} (\phi^2 - 1)^2 \right] \delta x dx \\ &\quad - \int_{\Omega} \gamma_2 (\nabla \psi \otimes \nabla \psi) \nabla \delta x dx - \int_{\Omega} \gamma_2 \nabla \frac{|\nabla \psi|^2}{2} \delta x dx.\end{aligned}$$

Here, ∇ denotes the gradient with respect to x .

Another integration by parts then gives

$$\begin{aligned}\delta E &= \int_{\Omega} \left[-\nabla W(\phi, \nabla \phi, \psi, \nabla \psi) \cdot \delta x - \left(\frac{\partial W}{\partial \nabla \phi} \otimes \nabla \phi + \frac{\partial W}{\partial \nabla \psi} \otimes \nabla \psi \right) : \nabla \delta x \right] dx \\ &= \int_{\Omega} -\nabla \cdot \left(W I - \frac{\partial W}{\partial \nabla \phi} \otimes \nabla \phi - \frac{\partial W}{\partial \nabla \psi} \otimes \nabla \psi \right) \delta x dx,\end{aligned}$$

where I is the identity matrix. The above gives the induced elastic force due to the interfacial mixing energy. Assuming the mixture of incompressible fluids such that $\nabla \cdot \delta x = 0$, the elastic stress tensor is uniquely determined up to an isotropic stress tensor, $f(x)I$. Therefore, the elastic stress tensor due to the mixing energy becomes

$$\sigma^e = W I - \frac{\partial W}{\partial \nabla \phi} \otimes \nabla \phi - \frac{\partial W}{\partial \nabla \psi} \otimes \nabla \psi + f(x)I.$$

We note that both isotropic tensors above can be absorbed into the pressure gradient term, which leads to the simplified equation

$$\tilde{\sigma}^e = -\frac{\partial W}{\partial \nabla \phi} \otimes \nabla \phi - \frac{\partial W}{\partial \nabla \psi} \otimes \nabla \psi = -\gamma_1 \varepsilon_1 \left(\frac{\psi - 1}{2} \right)^2 \nabla \phi \otimes \nabla \phi - \gamma_2 \varepsilon_2 \nabla \psi \otimes \nabla \psi.$$

We omit this dependence on tilde in the remainder of the paper, i.e., we use σ^e for the simplified stress tensor. We mention that a more precise definition of incompressibility is given by $J = \det \frac{\partial x}{\partial X} = 1$. Further, we note that a variation with respect to the domain can be used to account for this constraint, as discussed in [21].

Next, we add the dissipative terms to the system, namely the viscous stress tensor $\sigma^v = \frac{\nabla u + (\nabla u)^T}{2}$ with the viscosity coefficient μ . We also introduce the dissipation terms $\frac{\delta E}{\delta \phi}$ and $\frac{\delta E}{\delta \psi}$ into the convection relaxation equations for ϕ and ψ , with M_1 and M_2 denoting the rate coefficients for the relaxation at the interfaces. The resulting system of PDEs is now as follows

$$\rho (u_t + u \cdot \nabla u) + \nabla p = \lambda \nabla \cdot (\sigma^e + \sigma^v), \quad (2.4)$$

$$\phi_t + u \cdot \nabla \phi = -M_1 \frac{\delta E}{\delta \phi}, \quad (2.5)$$

$$\psi_t + u \cdot \nabla \psi = -M_2 \frac{\delta E}{\delta \psi}, \quad (2.6)$$

where

$$\frac{\delta E}{\delta \phi} = -\gamma_1 \left\{ \varepsilon_1 \nabla \cdot \left[\left(\frac{\psi - 1}{2} \right)^2 \nabla \phi \right] - \frac{1}{\varepsilon_1} \left(\frac{\psi - 1}{2} \right)^2 (\phi^2 - 1) \phi \right\},$$

and

$$\frac{\delta E}{\delta \psi} = -\gamma_2 \left\{ \varepsilon_2 \Delta \psi - \frac{1}{\varepsilon_2} (\psi^2 - 1) \psi \right\} + \gamma_1 \varepsilon_1 \frac{\psi - 1}{2} \left\{ \frac{1}{2} |\nabla \phi|^2 + \frac{1}{4\varepsilon_1} (\phi^2 - 1)^2 \right\}.$$

The above convection-relaxation equations (2.5) and (2.6) can be interpreted as a fastest descent method for the energy. Recall that the coefficients M_1 and M_2 determine the rates of the relaxation. The total system is thus dissipative with the governing energy law derived by multiplying (2.4) by u , (2.5) by $\frac{\delta E}{\delta \phi}$ and (2.6) by $\frac{\delta E}{\delta \psi}$, integrating and adding the results together, and then integrating by parts once again:

$$\frac{d\mathcal{E}}{dt} = - \int_{\Omega} \left(\mu |\nabla u|^2 + \lambda M_1 \left| \frac{\delta E}{\delta \phi} \right|^2 + \lambda M_2 \left| \frac{\delta E}{\delta \psi} \right|^2 \right) dx. \quad (2.7)$$

An *a priori* estimate of the solution then follows from the energy law:

$$\begin{aligned} u &\in L^\infty(0, T, L^2(\Omega)) \cap L^2(0, T, H^1(\Omega)) \\ \psi &\in L^\infty(0, T, H^1(\Omega)) \cap L^2(0, T, H^2(\Omega)) \end{aligned}$$

However, the regularity of ϕ can not be determined from the energy law because of the (possibly) degenerate pre-factor $(\psi - 1)^2/4$.

We understand that the relaxational equations (2.5) and (2.6) do not lead to the conservation of the order parameters ϕ and ψ . This issue can be solved by using the Cahn-Hilliard dynamics or a Lagrangian multiplier. As the main purpose of this paper is to introduce a mixing free energy for the three-phase mixture problem, we would like to leave the issue of order parameter conservation to our future works. In our numerical simulations, the rate coefficients M_1 and M_2 have been carefully chosen to control the violation of conservation.

Remark 2.1. *In simulations one can “turn off” the fluid by setting the velocity to zero in which case the motion is purely driven by mean curvature [5]. In similar ways, we can add other mechanisms to adapt to various models.*

Remark 2.2. *We mention that we can also set M_1 and M_2 to zero to reflect the pure transport kinematics. Analytical results on the zero Weissenberg number case can be found in [15] [14]. Although this case is of great interest in certain applications, simulation of the pure transport equation is beyond the scope of the current paper.*

3. Multi-phase simulations

In this section, we use numerical simulations to illustrate the applicability of our PFM for various multi-phase models.

3.1. Force Balance

To begin, we consider three different phases of materials as shown in Figure 1. In the absence of external forces and fluid effects, the dynamics of the system are driven purely by forces due to surface tensions induced from the mixing energy $E[\phi, \psi]$. An imbalance of forces at the three-phase contact line will thus drive the morphology until the forces are balanced. For example, if the surface tensions on the interfaces are equal, i.e. $\gamma_1 = \gamma_2$, then at equilibrium all three angles formed by the phases at the junction point are equal (120°).

To model this system numerically, we omit the fluid equations in (2.4) and use piecewise linear finite elements for the equations for ϕ, ψ spatially. Temporally, we use a fully implicit newton iteration. The discretized system is

$$\begin{aligned} \frac{\phi_h^{\text{new}} - \phi_h^n}{\Delta t} &= M_1 \gamma_1 \nabla \cdot \left[\left(\frac{\psi_h^n - 1}{2} \right)^2 \nabla \phi_h^{\text{new}} \right] \\ &\quad - M_1 \gamma_1 \frac{1}{\varepsilon_1^2} \left(\frac{\psi_h^n - 1}{2} \right)^2 \left[((\phi_h^{\text{old}})^2 - 1) \phi_h^{\text{old}} + (3(\phi_h^{\text{old}})^2 - 1) (\phi_h^{\text{new}} - \phi_h^{\text{old}}) \right], \\ \frac{\psi_h^{\text{new}} - \psi_h^n}{\Delta t} &= M_2 \gamma_2 \left[\Delta \psi_h^{\text{new}} - \frac{1}{\varepsilon_1^2} ((\psi_h^{\text{old}})^2 - 1) \psi_h^{\text{old}} - \frac{1}{\varepsilon_1^2} (3(\psi_h^{\text{old}})^2 - 1) (\psi_h^{\text{new}} - \psi_h^{\text{old}}) \right] \\ &\quad - M_2 \gamma_1 \left(\frac{\psi_h^{\text{new}} - 1}{2} \right) \left[\frac{1}{2} |\nabla \phi_h^n|^2 + \frac{1}{4\varepsilon_1^2} ((\phi_h^n)^2 - 1)^2 \right]. \end{aligned}$$

Here, Δt is the time step; ϕ_h^n and ψ_h^n are the finite element solutions at previous time steps t_n ; and $\phi_h^{\text{new}}, \phi_h^{\text{old}}, \psi_h^{\text{new}}$ and ψ_h^{old} are the Newton iterates at time step t_{n+1} . The discrete equations lead to symmetric yet possibly indefinite linear systems to solve at each time step for both ϕ and ψ . Our choice of solver is an ILU(0)-preconditioned GMRES method [19]. To track the moving interfaces throughout a simulation we use adaptive mesh coarsening and refinement [9]

based on the Kelly error estimator [11], defined as follows

$$e^2 = \sum_{i=1}^{N^h} \frac{h}{24} \int_{\partial\Omega_i^h} J^2 ds,$$

where J is the jump across the element boundary in the finite element approximation to the gradient. Here, $\{\Omega_i^h\}_{i=1}^{N^h}$ is the partition of the computational domain. In the simulation we compute the Kelly error estimator for the linear combinations of ϕ and ψ and refine those elements with the largest estimated errors that together make up 80 percent of the error and coarsen those cells of the error that account for a combined 10 percent of the smallest error (see Figure 3 for an illustration).

The computational domain in this simulation is $[0, 1] \times [0, 1]$, with the parameters set as $\mu = 1.0$, $\Delta t = 0.1$, $\varepsilon_1 = \varepsilon_2 = 0.01$, and $M_1 = M_2 = 0.001$. The surface tensions (γ_1, γ_2) are chosen as $(1.0, 1.0)$, $(1.5, 1.0)$ and $(1.0, 1.5)$ for three simulation cases. The initial conditions for the simulation are set as

$$\phi(x, y) = \begin{cases} -1 & x < 0.5 \\ +1 & x > 0.5 \end{cases} \quad \text{and} \quad \psi(x, y) = \begin{cases} -1 & y < 0.4 \\ +1 & y > 0.4 \end{cases}.$$

The results of three numerical tests for various choices of the surface tensions are provided in Figure 2. We note that, as expected, the angles between phases at the three-phase contact line increase as the surface tension decreases relative to its value on the other interfaces.

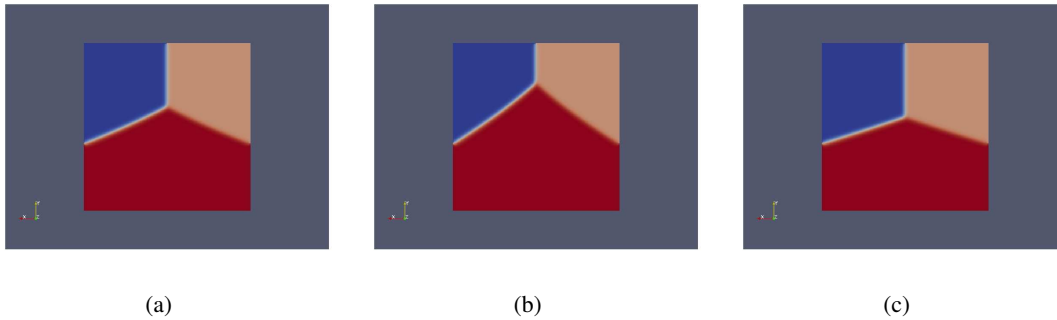


Figure 2: Force balance at the three-phase contact line in equilibrium for different choices of surface tensions γ_1 and γ_2 : 2(a): $\gamma_1 = \gamma_2 = 1.0$; 2(b): $\gamma_1 = 1.5$, and $\gamma_2 = 1.0$; 2(c): $\gamma_1 = 1.0$, and $\gamma_2 = 1.5$. In each case, the three dihedral angles and the three surface tensions (γ_1 , γ_2 , and γ_3) form a Neumann's triangle.

3.2. A Rising Bubble

The second application we consider is a model of a rising fluid bubble penetrating an interface formed by two different fluids. Here we label the fluid bubble by $\{\psi = 1\}$ and the region outside of it by $\{\psi = -1\}$. The two other fluids are then distinguished by an additional phase-field labeling function ϕ . We increase the densities of the outside fluids to induce a buoyancy which moves the bubble upward. Further, we mention that to avoid the complications that arise from variable densities, we adopt the Boussinesq approximation [16]. Additionally, we assume a low Reynolds number for the flow and thus replace the Navier-Stokes equations with the Stokes equations. With these simplifications, the multi-phase model reduces to

$$-\mu\Delta u + \nabla P = -\lambda \nabla \cdot \left\{ \tilde{\gamma}_1 \left(\frac{\psi - 1}{2} \right)^2 \nabla \phi \otimes \nabla \phi + \tilde{\gamma}_2 \nabla \psi \otimes \nabla \psi \right\} + f_{\text{bouss}}, \quad (3.1)$$

$$\nabla \cdot u = 0, \quad (3.2)$$

$$f_{\text{bouss}} = -(1 + \psi)(\rho_{\text{bubble}} - \rho_0)g - (1 - \psi)[(1 + \phi)(\rho_1 - \rho_0) + (1 - \phi)(\rho_2 - \rho_0)]g \quad (3.3)$$

Here, ρ_0 is the background density and its difference from the actual densities (ρ_{bubble} , ρ_1 , or ρ_2) gives rise to the buoyancy force, with ρ_{bubble} denoting the density of the fluid in the bubble and ρ_1 and ρ_2 denoting the densities of the other two fluids. The resulting system involves equations (2.5), (2.6), and (3.1) - (3.3). We discretize the Stokes system with Taylor-Hood finite elements [1], a well-known stable pair of elements for the velocity and pressure unknowns. The discretization then becomes

$$\left\langle \left(1 + \frac{\Delta t M_1 \gamma_1}{\varepsilon_1^2} (3(\phi_h^{\text{old}})^2 - 1) \left(\frac{\psi_h^n - 1}{2} \right)^2 \right) \phi_h^{\text{new}}, \eta \right\rangle + \left\langle \Delta t M_1 \gamma_1 \left[\left(\frac{\psi_h^n - 1}{2} \right)^2 \nabla \phi_{n+1} \right], \nabla \eta \right\rangle$$

$$+ \left\langle \Delta t (u_h^n \cdot \nabla \phi_h^{\text{new}}), \eta \right\rangle = \left\langle \phi_n - \frac{\Delta t M_1 \gamma_1}{\varepsilon_1^2} \left(\frac{\psi_h^n - 1}{2} \right)^2 (2(\phi_h^{\text{old}})^3) \eta \right\rangle,$$

$$\left\langle \left[1 + \frac{\Delta t M_2 \gamma_2}{\varepsilon^2} (3(\psi_h^{\text{old}})^2 - 1) + \frac{1}{2} \Delta t M_2 \gamma_1 \left(\frac{1}{2} |\nabla \phi|^2 + \frac{1}{4\varepsilon_1^2} (\phi^2 - 1)^2 \right) \right] \psi_h^{\text{new}}, \eta \right\rangle$$

$$+ \left\langle \Delta t M_2 \gamma_2 \nabla \psi_{n+1}, \nabla \eta \right\rangle + \left\langle u_h^n \cdot \psi_h^{\text{new}}, \eta \right\rangle$$

$$= \left\langle \psi_h^n + \frac{\Delta t M_2 \gamma_2}{\varepsilon_1^2} (2(\psi_h^{\text{old}})^3) + \frac{\Delta t M_2 \gamma_1}{2} \left[\frac{1}{2} |\nabla \phi_h^n|^2 + \frac{1}{4\varepsilon_1^2} ((\phi_h^n)^2 - 1)^2 \right], \eta \right\rangle,$$

$$\mu \left\langle \nabla u_h^n, \nabla w \right\rangle + \left\langle \nabla p_h^n, w \right\rangle = \left\langle \lambda \left(\left(\frac{\psi_h^n - 1}{2} \right)^2 \nabla \phi_h^n \otimes \nabla \phi_h^n + \nabla \psi_h^n \otimes \nabla \psi_h^n \right), \nabla w \right\rangle + \left\langle f_{\text{ext}}, w \right\rangle,$$

and

$$\left\langle \nabla \cdot u_h^n, q \right\rangle = 0.$$

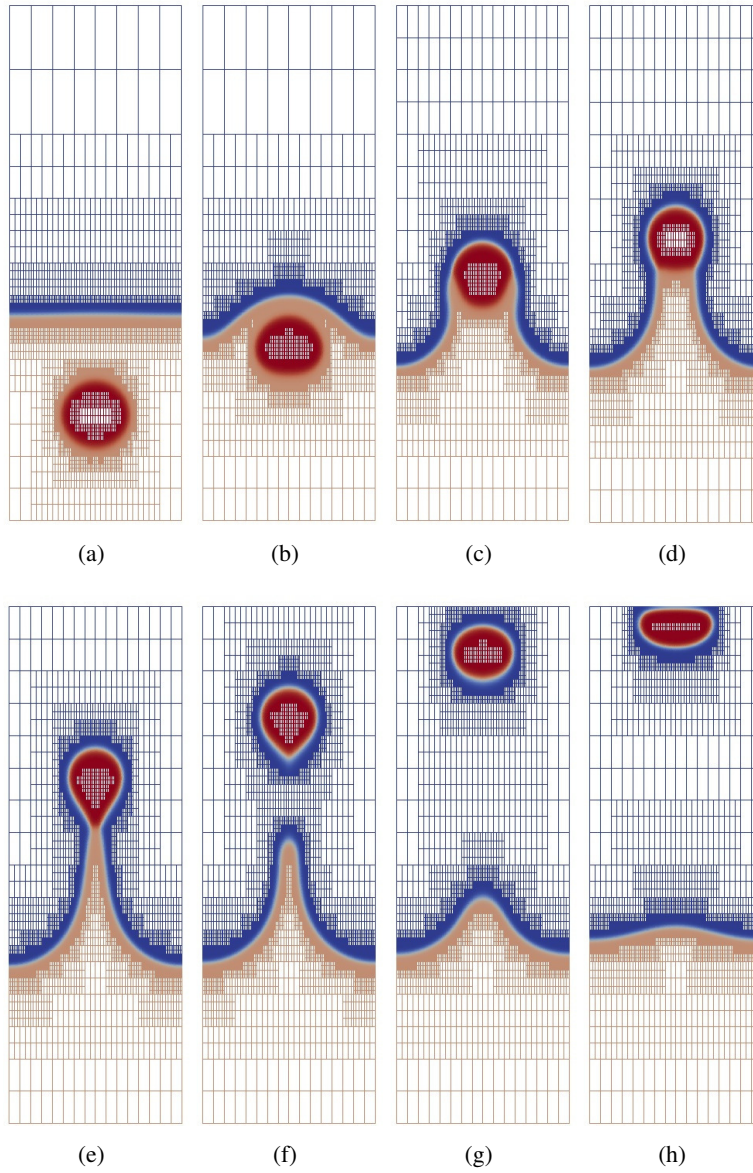


Figure 3: Rise of a fluid bubble ($\psi = 1$) that penetrates a fluid-fluid interface ($\phi = 0$ and $\psi = -1$). The computational domain is $[0, 1] \times [0, 3]$ in all the eight subplots. The adaptive mesh refinement and coarsening for the Kelly error estimator are plotted as well.

where w is a **P2** test function and q and η are **P1** test functions.

Permuting the equations such that the pressure unknowns appear after the velocities, the stiffness matrix for Stokes equations has the following block structure

$$\begin{pmatrix} A & B^T \\ B & 0 \end{pmatrix} \begin{pmatrix} u \\ p \end{pmatrix} = \begin{pmatrix} f \\ g \end{pmatrix}.$$

A step of block Gaussian Elimination then gives

$$\begin{aligned} BA^{-1}B^T p &= BA^{-1}f - g, \\ Au &= f - B^T p. \end{aligned}$$

The Pressure Schur Complement of the system $S = BA^{-1}B^T$ ([22]) then plays the central role in the linear algebra. Fortunately, the discrete Laplacian operator A is symmetric and positive definite and B has full row rank, an observation that leads to a variety of effective preconditioners for this system. Our basic solver consists of the following block preconditioner for GMRES iterations:

$$P = \begin{pmatrix} A & 0 \\ B & -S \end{pmatrix},$$

or equivalently

$$P^{-1} = \begin{pmatrix} A^{-1} & 0 \\ S^{-1}BA^{-1} & -S^{-1} \end{pmatrix},$$

so that

$$P^{-1} \begin{pmatrix} A & B^T \\ B & 0 \end{pmatrix} = \begin{pmatrix} I & A^{-1}B^T \\ 0 & I \end{pmatrix}.$$

We note that this preconditioner is attractive as it reduces the task of inversion of an indefinite system to that of solving symmetric and positive definite systems with smaller problem sizes. Of course, direct inversion of A is impractical and thus we use a mass matrix M_p instead in defining the preconditioner.

The parameters of our tests are set as follows: $\Delta t = 0.01$, $\gamma_1 = \gamma_2 = 0.1$, $g = (0, 40)^T$, $\lambda = 0.01$, $M_1 = M_2 = 0.001$, $\rho_{\text{bubble}} - \rho_0 = 1$, and $\rho_1 = \rho_2 = \rho_0$. The gravitational force g is assigned a large value because the Allan-Cahn dynamics of our model do not preserve the volumes of the phases. Generally, the diffusion effect will eventually cause the bubble to shrink over time. This shrinking effect can be controlled numerically by increasing g ([16]), i.e., by reducing the elapsed time in the numerical experiment.

Figure 3 shows the upward motion of a fluid bubble ($\psi = 1$) that penetrates a fluid-fluid interface ($\phi = 0$ and $\psi = -1$). The computational domain is $[0, 1] \times [0, 3]$ in all the eight subplots. Subplot 3(a) shows the initial configuration, where the bubble is immersed in the lower fluid, the fluid-fluid interface is horizontal, and all the fluids are at rest. Subplot 3(b) shows that the fluid-fluid interface is displayed by the approaching bubble in drift motion. Accompanying the continuous rise of the bubble, the interface breaks to two pieces, with two three-phase contact lines formed at the surface of the bubble, as shown in subplot 3(c). These two three-phase contact lines then move downward relative to the surface of the rising bubble, as shown in subplots 3(d) and 3(e). It is observed that in this stage, the bubble exhibits appreciable deformation, a manifestation of viscoelasticity that arises from a balance between viscous and capillary forces. Subplots 3(e) and 3(f) show that the two three-phase contact lines merge as they both reach the stretched bottom of the bubble. Consequently, the fluid-fluid interfaces, once separated by the intervening bubble, are joined to form one interface, which is immediately detached from the bubble. After this pinch off, the bubble continues to rise in the upper fluid, with a reduced deformation due to the detachment of the three-phase contact lines from the bubble surface,

as shown in subplots 3(f) and 3(g). Meanwhile, the surface tension of the fluid-fluid interface drives it toward the initial (horizontal) profile. In the last subplot 3(h), the fluid-fluid interface is already very close to its initial profile, while the bubble, with its upward motion stopped by the impermeable boundary, shows an expected deformation.

3.3. Investigation of slip

As a last application, we incorporate slip effects into a simulation. Traditionally, the slip phenomena has been accounted for by specifying certain boundary conditions. For example, the following Stokes equations with the so-called Navier boundary condition [13]

$$-\mu \Delta u + \nabla p = 0 \quad \text{in } \Omega, \quad (3.4)$$

$$2\mu\epsilon(u)_{n\tau} = \beta u_\tau^{slip} \quad \text{on } \partial\Omega, \quad (3.5)$$

can be formulated as the following variational problem [18]

$$\min_{u,p} \left\{ \int_{\Omega} 2\mu\epsilon(u) : \epsilon(u) dx + \int_{\partial\Omega} \beta (u_\tau^{slip})^2 dS \right\}, \quad (3.6)$$

where $\epsilon(u) = \frac{\nabla u + (\nabla u)^T}{2}$ is the symmetric part of the velocity gradient. Hence, we can see that the slip boundary conditions contribute to the dissipation functional. In our diffuse interface model, we assume slip is induced by a thin layer (a diffuse interface associated with one of the labeling functions, say ψ) of nearly inviscid fluid that surrounds a solid, as depicted in Figure 4.

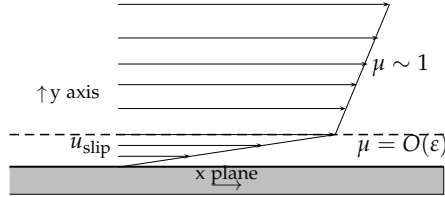


Figure 4: A schematic illustration for fluid slipping modeled by a fast variation of tangential velocity across a thin layer (diffuse interface) with a small viscosity.

Formally, we can show that our assumption of a thin layer on a flat plane can approximate the boundary value problem given by (3.4) and (3.5) in terms of the associated energy as follows. The bulk energy dissipation functional is given by

$$\int_{\Omega} 2\mu\epsilon(u) : \epsilon(u) dx.$$

We assume that in the thin layer illustrated in the picture we have the following velocity profile

$$\begin{aligned} u_\tau(x, y) &= \frac{y}{\epsilon} u_\tau^{slip}(x), \\ u_n(x, y) &= 0, \end{aligned}$$

and that the viscosity is proportional to the interfacial width ε :

$$\mu = \beta\varepsilon$$

in the thin layer. Then the energy dissipation in the thin layer reduces to

$$\int_{xplane} \int_0^\varepsilon \beta\varepsilon \left(\frac{u_\tau^{slip}(x)}{\varepsilon} \right)^2 dy dS(x) = \int_{xplane} \beta(u_\tau^{slip})^2 dS(x)$$

which is the same as the slip contribution in (3.6). Therefore, asymptotically (with respect to ε) the diffuse interface model with small viscosity inside the interface approximates the traditional sharp interface model energetically.

We next consider the effects of our diffuse interface model for slip in an application of a solid ball dropping into a two-phase Stokesian flow. We distinguish the solid and fluid by ψ and the fluids by ϕ . The solid behavior is achieved by assuming a large bulk viscosity in the solid ball. In our implementation, we take

$$\mu(\psi) = \begin{cases} 30 & \psi = 1 \\ 1 & \psi = -1 \\ \varepsilon_2 & |\psi| < 1 \end{cases},$$

where the larger value of the viscosity ($\mu = 30$) is used to model the solid phase and the smaller ($\mu = \varepsilon_2$) is used to produce the slip effect.

Mathematically, our assumption on viscosity only changes the PDEs of the model slightly to the tensor formulation of the Stokes equations:

$$2\nabla \cdot (\mu(\psi)\varepsilon(u)) + \nabla p = \nabla \cdot \sigma^e(\phi, \nabla\phi, \psi, \nabla\psi).$$

Numerically, we can thus continue to use an AMG preconditioner based on the stiffness matrix $\langle \mu(\psi)\nabla u, \nabla w \rangle$, which is spectrally equivalent to the tensor formulation $\langle 2\mu(\psi)\varepsilon(u), \varepsilon(w) \rangle$.

Numerical simulations have been carried out for a solid particle that is falling in a two-phase Stokesian flow with and without slip at the solid surface. The results for a slippery particle are shown in Figure 5 and those for a non-slippery particle are in Figure 6. It is clearly observed that a slippery surface leads to a more rapid ‘‘pinch-off’’ of the upper fluid from the solid particle. Physically, two contact lines are formed as soon as the falling particle touches the fluid-fluid interface. Accompanying the fall of the particle, the contact lines gradually move upward relative to the solid surface. According to the Onsager principle of least energy dissipation [18], fluid slip would facilitate the contact line motion relative to the solid surface. The faster moving contact lines at the slippery surface then lead to an earlier arrival at the top of the particle and consequently a more rapid pinch-off. This also explains the observation that during the moment of penetrating the fluid-fluid interface, there is more upper fluid wrapping the non-slippery particle with slower moving contact lines. To summarize, these observations are consistent with the Onsager principle of least energy dissipation as fluid slip provides a mechanism to reduce the total rate of dissipation.

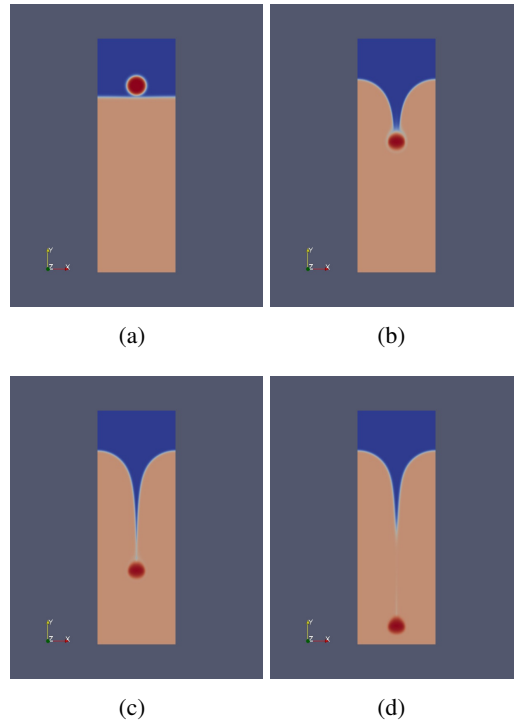


Figure 5: A solid particle with a slippery surface falling in a binary fluid. Contact lines are formed upon the impact of the particle on the fluid-fluid interface. Accompanying the fall of the particle, the contact lines quickly move upward relative to the particle surface. Upon their arrival at the top of the particle, there is a pinch-off.

4. Concluding remarks

We introduced a diffuse interface model to describe the three-phase dynamics using two phase field variables. The model can be derived through a variational approach to both the conservative and the dissipative parts of the dynamics. The applicability of the model has been demonstrated through simulations for (1) the force balance at the three-phase contact line in equilibrium, (2) a rising bubble penetrating a fluid-fluid interface, and (3) a solid particle falling in a binary fluid, with fluid slip at solid surface taken into account. An interesting application of the present model is to further investigate the effect of particle surface wettability on the impact of the solid particle on a fluid-fluid interface [8]. For this purpose, the free energy functional needs to be generalized to model the different wettabilities of the two fluid phases on the third (solid) phase. Work in this direction is currently underway.

The applicability of the model was demonstrated by numerical results that focused on simplified two dimensional models of various multi-phase materials. Future work in this direction concerns the development of a three-dimensional parallel code. This in turn requires further improvements to the numerical models and the numerical algorithms used for approximating the coupled nonlinear systems of PDEs.

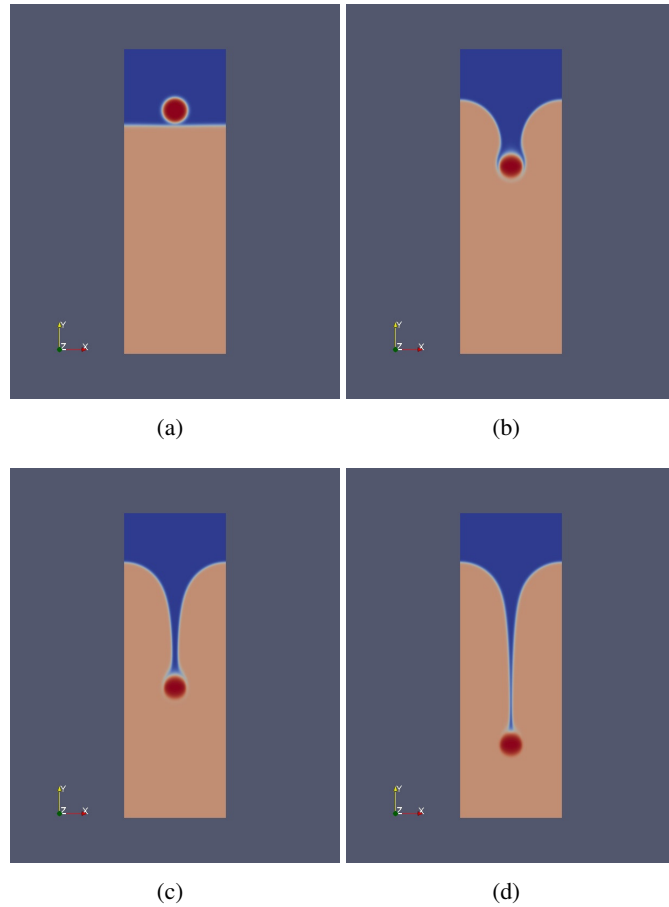


Figure 6: A solid particle with a non-slippery surface falling in a binary fluid. Compared to Figure 5, here the contact line motion is relatively slow. Consequently, the particle is wrapped by more upper fluid in the early stage of penetration and the pinch-off occurs at a larger depth (not shown).

Acknowledgements. Brannick's work was partially supported by grant NSF-DMS 1320608. Liu's work was partially supported by grant NSF DMS-1109107. Sun would like to thank the Institute for Mathematics and Its Applications (IMA) and Hong Kong University of Science and Technology as a considerable amount of his work is done during his visits to the two institutes.

References

- [1] F. Brezzi and M. Fortin. *Mixed and Hybrid Finite Element Methods*. Number 15 in Computational Mathematics. Springer-Verlag, 1991.
- [2] Lia Bronsard, Changfeng Gui, and Michelle Schatzman. A three-layered minimizer in r^2 for a variational problem with a symmetric three-well potential. *Comm. Pure and Applied Math.*,

- XLIX(673), 1996.
- [3] J. W. Cahn and J. E. Hillard. Free energy of a nonuniform system. I. Interfacial free energy. *J. Chem. Phys.*, 28:258–267, 1958.
 - [4] M. Doi and S. F. Edwards. *The Theory of Polymer Dynamics*. Oxford Science Publication, 1986.
 - [5] Q. Du, C. Liu, R. Ryham, and X. Wang. Modeling the spontaneous curvature effects in static cell membrane deformations by a phase field formulation. *Communications on Pure and Applied Analysis*, 4:537 – 548, 2005.
 - [6] Q. Du, C. Liu, R. Ryham, and X. Wang. The phase field formulation of the willmore problem. *Nonlinearity*, 18:1249 – 1267, 2005.
 - [7] Q. Du, C. Liu, and X. Wang. A phase field approach in the numerical study of the elastic bending energy for vesicle membranes. *Journal of Computational Physics*, 198(2):450–468, 2004.
 - [8] C. Duez, C. Ybert, C. Clanet, and L. Bocquet. Making a splash with water repellency. *Nature Physics*, 3(180), 2007.
 - [9] W. Huang, Y. Ren, and R. D. Russell. Moving mesh partial differential equations (mmpdes) based on the equidistribution principle. *SIAM J. Numer. Anal.*, 31:709–730, 1994.
 - [10] J.S. Lowengrub J.S. Kim. Phase field modeling and simulation of three-phase flows. *Interfaces Free Bound*, 7:435–466, 2005.
 - [11] D. W. Kelly, J.P. Gago, O.C. Zienkiewicz, and I. Babuska. A posteriori error analysis and adaptive proces in the finite element method: part i – error analysis. *International Journal for Numerical Methods in Engineering*, 19:1593–1619, 1983.
 - [12] Junseok Kim. Phase field computations for ternary fluid flows phase field computations for ternary fluid flows. *Computer Methods in Applied Mechanics and Engineering*, 196(45):4779–4788, 2007.
 - [13] H. Lamb. *Hydrodynamics*. Cambridge, 6th edition, 1932.
 - [14] Zhen Lei, Chun Liu, and Yi Zhou. Global solutions for incompressible viscoelastic fluids. *Arch. Rational Mech. Anal.*, 188, 2008.
 - [15] F. H. Lin, C. Liu, and P. Zhang. On a micro-macro model for polymeric fluids near equilibrium. *Comm. Pure Appl. Math.*, LIX:1–29, 2005.
 - [16] C. Liu and J. Shen. A phase field model for the mixture of two incompressible fluids and its approximation by a fourier-spectral method. *Physica D*, 179:211–228, 2003.
 - [17] T. Qian, X. P. Wang, and P. Sheng. Molecular scale contact line hydrodynamics of immiscible flows. *Phys. Rev. E*, 68(016306), 2003.
 - [18] T. Qian, X. P. Wang, and P. Sheng. A variational approach to the moving contact line hydrodynamics. *J. Fluid Mech.*, 564:333 – 360, 2006.
 - [19] S. S. Eisenstat, H. Elman, and M. Schultz. Variational iterative methods for nonsymmetric systems of linear equations. *SIAM J. of Num. Anal.*, 20(2):345–357, 1983.
 - [20] Jie Shen and Xiaofeng Yang. A phase-field model and its numerical approximation for two-phase incompressible flows with different densities and viscosities. *SIAM J. Sci. Computing*, 32(1159), 2010.
 - [21] H. Sun and C. Liu. On energetic variational approaches in modeling the nematic liquid crystal flows. *DCDS-A*, 23:455–475, 2008.
 - [22] Stefan. Turek. *Efficient solvers for incompressible flow problems : an algorithmic and computational approach*. Springer, 1999.
 - [23] P. Yue, J. Feng, C. Liu, and J. Shen. A diffuse-interface method for simulating two-phase flows of complex fluids. *Journal of Fluid Mechanics*, 515:293–317, 2005.